# Three-Dimensional Polarization Control in Microscopy

Ayman F. Abouraddy[1,*] and Kimani C. Toussaint, Jr.[2]

[1]*Research Laboratory of Electronics, Massachusetts Institute of Technology, Cambridge, Massachusetts 02139, USA*
[2]*The James Franck Institute, University of Chicago, Chicago, Illinois 60637, USA*

We propose an approach to optical microscopy that enables full control over the three-dimensional polarization vector at the focal spot of a high-numerical-aperture lens. The input field to the lens is linearly polarized and no polarization optics are needed. This technique utilizes the *azimuthal* spatial degree of freedom of the input field. We find that only a small set of low-order azimuthal spatial harmonics contributes to the focused field on axis, and a simple transformation exists between the linear vector space of these harmonics and the three-dimensional polarization-vector space. Controlling the relative complex weights of these azimuthal harmonics produces any desired three-dimensional state of polarization.

Although control over the spatial distribution of an optical field focused by a lens is a well-established endeavor [1,2], full control over the polarization of the focused field has only recently attracted attention [3]. A microscope that delivers a tunable 3D state of polarization to the focus will have tremendous impact on several fundamental and applied fields of research. For example, determining the orientation of the absorption dipole moment of single molecules is currently an indirect process whereby image processing is used to deduce the information [4]. Probing such systems with a controllable 3D polarization focal field, however, would enable direct determination of the dipole moment, thereby increasing both the speed and accuracy of these measurements. Another example is field-enhanced measurements using metallic nanoprobes, in both linear and nonlinear imaging modalities [5]. These techniques are of considerable interest because of the resulting sub-diffraction-limited resolution, but are complicated by the requirement of precisely aligning the apex of the nanoprobe tip with the peak of the local longitudinally *z*-polarized focal field. Tuning the 3D state of polarization in the focal spot would allow precise delivery of a *z*-polarized field thereby mitigating this obstacle. Another avenue that would benefit from such a microscope is quantum control of chemical-interaction pathways that have been found to be sensitive to the polarization of probing femtosecond pulses [6]. Furthermore, a method for enantiomeric enrichment of chiral molecules has recently been proposed [7], whereby one field component is used for orientation and the other two are used for chirality control, but has not hitherto been demonstrated since approaches to controlling 3D polarization are not available. Controlling the 2D polarization of a focused optical field has recently been used to apply a precise torque to trapped particles [8] and to facilitate the study of DNA molecules and biological molecular motors [9]. Controlling the 3D polarization would obviously further the capabilities of such a scheme.

In this Letter we present an approach to optical microscopy that delivers any desired *3D state of polarization* to the focus of a high-numerical-aperture (high-NA) lens. We find, surprisingly, that one does not need to change the input polarization to achieve this. Although the input field used is linearly polarized, the *polarization* at the focal spot is tuned through sculpting the *scalar* complex field distribution in the *azimuthal* direction. We find that only certain low-order azimuthal spatial harmonics are focused onto the optical axis, and we identify three harmonics each of which produces a linearly polarized component. The radial distribution of the input beam, on the other hand, determines the resolution of the focused field. The formalism we introduce elucidates the underlying principles that govern the behavior of focused "vector beams" [3], i.e., beams that are nonuniformly polarized. Indeed, their interesting features can be understood in terms of the azimuthal spatial content of their linearly polarized components. The system that we consider is the traditional epi-illumination microscope [2].

The fundamental equation, derived by Richards and Wolf [10], that describes a monochromatic field **E** at **r** = $(\rho, \psi, z)$ in the vicinity of the geometric focal point of a high-NA lens (focal length $f$, the optical axis is the $z$ axis) for a linearly polarized input field is

$$\mathbf{E}(\mathbf{r}) = \frac{-ik}{2\pi} \int_0^{2\pi} d\beta \int_0^{\theta_1} d\alpha A(\alpha, \beta) \sin\alpha \, \mathbf{p}(\alpha, \beta) e^{i\mathbf{k}\cdot\mathbf{r}},$$
(1)

where $k = \frac{2\pi}{\lambda}$, $\alpha$ and $\beta$ are the altitude and azimuthal angles, respectively, with respect to the geometric focal point and the optical axis, the exponent is given by $\mathbf{k}\cdot\mathbf{r} = k[z\cos\alpha - \rho\sin\alpha\cos(\beta - \psi)]$, and $\theta_1$ is the half-cone angle subtended by the lens at the focal point [see Fig. 1(a) for a schematic of the geometry]. The unit vector $\mathbf{p}(\alpha, \beta)$, which depends only on the input polarization, represents the scattering from the input-field polarization into other polarizations by virtue of the lens curvature, and
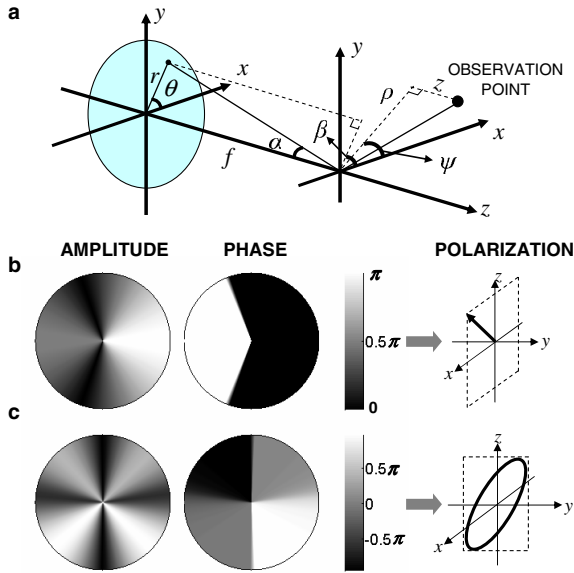
FIG. 1 (color online). (a) Schematic of the focusing geometry showing the input plane and an observation point in the vicinity of the focal point. (b),(c) Examples of input-field distributions designed to produce desired 3D states of polarization at the focal spot: amplitude and phase distributions of the $x$-polarized input field needed to produce (b) 45° linear polarization in the $x$-$z$ plane, and (c) elliptical polarization in the $y$-$z$ plane.

for an $x$-polarized input field $\mathbf{p}^{\mathrm{T}}(\alpha, \beta) = [\cos\alpha + (1 - \cos\alpha)\sin^2\beta, -(1 - \cos\alpha)\sin\beta\cos\beta, \sin\alpha\cos\beta]$. For an immersion lens $\mathrm{NA} = n\sin\theta_1$, where $n$ is the index of refraction of the immersion fluid (in this Letter, $n = 1.5$). The input field $E_o(r, \theta)$ to an aplanatic lens obeying the Abbe sine condition is related to $A(\alpha, \beta)$ by $A(\alpha, \beta) = E_o(f\sin\alpha, \beta)\sqrt{|\cos\alpha|}$ [1], where $\alpha$ and $\beta$ thus represent the radial and azimuthal variables, respectively.

To study the effect of the input-field spatial distribution on the polarization of the focused spot, we need to explore the full space of 2D complex functions $A(\alpha, \beta)$, which is doubly infinite in dimension. However, it is known that (under very general conditions) any arbitrary distribution $A(\alpha, \beta)$ may be written in the form of a superposition of separable products known as the Schmidt decomposition [11]: $A(\alpha, \beta) = \sum_j \eta_j \Gamma_j(\alpha)\Lambda_j(\beta)$, where the coefficients $\eta_j$ are real numbers. In order to obtain analytical insight, we confine ourselves to investigating a special class of distributions that have a single term in the Schmidt decomposition $A(\alpha, \beta) = \Gamma(\alpha)\Lambda(\beta)$, i.e., fields that are separable in the radial and azimuthal directions. Although seemingly a restrictive assumption, all beams that have been considered heretofore in microscopy belong to a *subset* of this class, namely, distributions having circular symmetry.

Since the support of the function $\Lambda(\beta)$ is the interval $[0, 2\pi)$, we use a Fourier-series representation,

$$\Lambda(\beta) = \bar{\Lambda} + \sum_{n=1}^{\infty}\{C_n \cos n\beta + S_n \sin n\beta\}, \quad (2)$$

where $\cos n\beta$ and $\sin n\beta$ are azimuthal spatial harmonics. By placing $C_n = S_n = 0$, $n \geq 1$ (i.e., $\Lambda(\beta) = \bar{\Lambda}$), we retrieve the familiar results [1] that assume a circularly symmetric input-beam distribution. It is this assumption that masks the rich behavior of the azimuthal harmonics. Setting $z = 0$ in Eq. (1) and substituting from Eq. (2), we obtain the field polarization components in the focal plane. We find that only a few of these harmonics are useful for our goal of controlling the 3D state of polarization of the focused light [12]. In fact only the $\bar{\Lambda}$, $C_1$, $C_2$, and $S_2$ harmonics contribute to the focal field on axis (i.e., having the peak of their contribution at $\rho = 0$). All higher-order harmonics ($n > 2$), together with the $\sin\beta$ harmonic, do *not* contribute to the on-axis field (but give rise to features lying away from the optical axis), and hence we remove them from the set of input-field distributions that we study. Moreover, we find that the on-axis $x$-polarized component arises from both the $\bar{\Lambda}$ and $C_2$ harmonics, the $y$ polarization from the $S_2$, and the $z$ polarization from the $C_1$. We remove the $C_2$ harmonic, which is redundant for our task, and study input fields having the azimuthal distribution

$$\Lambda(\beta) = \bar{\Lambda} + S_2 \sin 2\beta + C_1 \cos\beta. \quad (3)$$

The functions $\{1, \sin 2\beta, \cos\beta\}$ form an orthogonal basis (under the usual inner product) for a 3D linear vector space, and the function $\Lambda(\beta)$ is a vector having coordinates $(\bar{\Lambda}, S_2, C_1)$.

The field components in the focal plane can now be expressed in the form of a superposition of contributions from these azimuthal spatial harmonics, separated into two classes: contributions to the *on-axis* field (incorporated into a linear transformation $\mathbf{M}_{\mathrm{on\text{-}axis}}$) and contributions that lie *away from the axis* ($\mathbf{M}_{\mathrm{off\text{-}axis}}$):

$$\begin{pmatrix} E_x(\rho, \psi) \\ E_y(\rho, \psi) \\ E_z(\rho, \psi) \end{pmatrix} = \{\mathbf{M}_{\mathrm{on\text{-}axis}}(\rho) + \mathbf{M}_{\mathrm{off\text{-}axis}}(\rho, \psi)\}\begin{pmatrix} \bar{\Lambda} \\ S_2 \\ C_1 \end{pmatrix}, \quad (4)$$

where

$$\mathbf{M}_{\mathrm{on\text{-}axis}}(\rho) = \begin{pmatrix} I_0^a(\rho) & 0 & 0 \\ 0 & -\frac{1}{2}I_0^b(\rho) & 0 \\ 0 & 0 & \frac{1}{2}I_0^c(\rho) \end{pmatrix} \quad (5)$$

and

$$\mathbf{M}_{\mathrm{off\text{-}axis}}(\rho, \psi) = \begin{pmatrix} I_2^b(\rho)\cos 2\psi & -I_2^a(\rho)\sin 2\psi - \frac{1}{2}I_4^b(\rho)\sin 4\psi & i\{I_1^a(\rho) - \frac{1}{2}I_1^b(\rho)\}\cos\psi + \frac{i}{2}I_3^b(\rho)\cos 3\psi \\ I_2^b(\rho)\sin 2\psi & \frac{1}{2}I_4^b(\rho)\cos 4\psi & \frac{i}{2}\{-I_1^b(\rho)\sin\psi + I_3^b(\rho)\sin 3\psi\} \\ iI_1^c(\rho)\cos\psi & \frac{1}{2}\{I_1^c(\rho)\sin\psi - I_3^c(\rho)\sin 3\psi\} & -\frac{1}{2}I_2^c(\rho)\cos 2\psi \end{pmatrix}. \quad (6)$$

The functions $I_n^\Omega(\rho)$, $\Omega = a, b, c$, are given by

$$I_n^\Omega(\rho) = \frac{-ik}{2} \int_0^{\theta_1} d\alpha \Gamma(\alpha) H^\Omega(\alpha) J_n(-\rho k \sin\alpha), \quad (7)$$

where $H^a(\alpha) = \sin\alpha(1 + \cos\alpha)$, $H^b(\alpha) = \sin\alpha(1 - \cos\alpha)$, and $H^c(\alpha) = 1 - \cos2\alpha$; $J_n$ is the $n$th order Bessel function of the first kind. Examining the behavior of the functions $I_n^\Omega(\rho)$ provides the justification for grouping the various terms in the transformations $\mathbf{M}_{\text{on-axis}}$ and $\mathbf{M}_{\text{off-axis}}$. Since $J_0(x)$ has its peak at $x = 0$, while $J_n(x)$ ($n \geq 1$) peaks away from $x = 0$, one can verify that $I_0^a$, $I_0^b$, and $I_0^c$ have their peaks at $\rho = 0$, while $I_n^a$, $I_n^b$, and $I_n^c$ ($n \geq 1$) peak away from $\rho = 0$. Equations (4) and (5) thus show that the $\bar{\Lambda}$, $S_2$, and $C_1$ harmonics produce on-axis $x$, $y$, and $z$-polarized components, respectively. Note that $\mathbf{M}_{\text{on-axis}}$ is independent of $\psi$, and hence the on-axis contributions of the three harmonics are circularly symmetric, whereas their off-axis contributions are not.

In general, moving in the parameter space of azimuthal-spatial-harmonics coefficients results in tuning the 3D state of polarization at the focal spot. We need only account for the ratios of the peak values, $I_0^a(0)$, $I_0^b(0)$, and $I_0^c(0)$, which depend on the NA of the lens and the radial distribution of the input field $\Gamma(\alpha)$. For example, an input field having a uniform radial distribution and a lens with NA = 1.3 results in $I_0^b(0)/I_0^a(0) = 0.135$ and $I_0^c(0)/I_0^a(0) = 0.679$. Hence, in order to produce a 45°-linear polarization in the $x$-$z$ plane in this case, the required coefficients for the azimuthal spatial harmonics are $(\bar{\Lambda}, S_2, C_1) = (1, 0, 3)E_o$, with $E_o$ an arbitrary constant; the amplitude and phase distributions of this field are depicted in Fig. 1(b). Choosing the coefficients $(0, 1, 0.34e^{-i(3/4)\pi})E_o$ for the input field [see Fig. 1(c)] results in a focused spot having elliptical polarization in the $y$-$z$ plane on the optical axis, despite the fact that the input beam is $x$ polarized.

Although it is known that the most general state of 2D polarization (for TEM and paraxial waves) is elliptical, it is not obvious *a priori* what the most general counterpart for 3D polarization might be, where the tip of the electric field vector traces a periodic curve in 3D characterized by *4 parameters* (2 relative amplitudes and 2 relative phases). It turns out, however, that the most general 3D state of polarization is still elliptical, albeit with the plane of the ellipse tilted in space [12]. An example is given in Fig. 2(a) where the projected polarization of the field in the focal spot is elliptical in the $x$-$y$ plane, circular in the $y$-$z$ plane, and linear in the $x$-$z$ plane. The field components of this focused field are $(E_x, E_y, E_z) \propto (5, i\sqrt{3}, \sqrt{3})$, which may be produced by an $x$-polarized input field having a uniform radial distribution and azimuthal coefficients $(\bar{\Lambda}, S_2, C_1) = (1, i5.2, 1)E_o$ focused with an NA = 1.3 lens. The amplitude and phase distributions of the input field required to produce this 3D polarization state are shown in Fig. 2(b).

The separation of the radial and azimuthal variables helps shed light on another issue, namely, that the resolution of the on-axis focal spot is not determined by the

azimuthal distribution of the input field, only by its radial dependence $\Gamma(\alpha)$ through the functions $I_n^a$, $I_n^b$, and $I_n^c$. Thus, after choosing the coefficients of the azimuthal spatial harmonics to obtain the required 3D state of polarization, one then designs the radial distribution $\Gamma(\alpha)$ to specify the focal spot distribution [13].

In order to appreciate the usefulness of vector beams at the input to the lens for control of the polarization at the focal point, we consider the conversion efficiencies from these three azimuthal harmonics to the three focused polarization components. For an $x$-polarized input field having a uniform radial distribution (NA = 1.3), the $\bar{\Lambda}$ harmonic results in 70.2% of the input power transferred to the on-axis $x$ component, while the rest of the power is transferred to the off-axis $x$, $y$, and $z$ field components. The $C_1$ harmonic transfers 20.2% of the power to on-axis $z$ component, while 10.1% is in the off-axis $z$ component. As expected from the $I_0^b(0)/I_0^a(0)$ ratio given above, the conversion is lowest from the $S_1$ harmonic to the $y$ component (only 1%). There are two approaches to the optimization of these conversion ratios. The first is through the design of the input-field *radial* spatial distribution and the lens NA [12], which can lead to a considerable alteration of these conversion efficiencies. The second approach is the use of a vector beam in lieu of a scalar one, especially in order to produce a $y$-polarized component efficiently, as we proceed to show.

We generalize our approach by including a $y$-polarized component in the input field, resulting in a *vector* beam. Revisiting Eq. (1), the polarization vector $\mathbf{p}(\alpha, \beta)$ for a $y$-polarized input field is $\mathbf{p}^T(\alpha, \beta) = [-(1 - \cos\alpha) \times \sin\beta \cos\beta, \cos\alpha + (1 - \cos\alpha)\cos^2\beta, \sin\alpha \sin\beta]$, and the azimuthal distribution relevant to our goal is

$$\Lambda_y(\beta) = S_2^y \sin2\beta + \bar{\Lambda}^y + S_1^y \sin\beta, \quad (8)$$

with these $y$-polarized harmonics producing on-axis polarization components in accordance to $(S_2^y, \bar{\Lambda}^y, S_1^y) \Rightarrow (E_x, E_y, E_z)$. To produce a 3D linearly polarized beam having $E_x = E_y = E_z$, one can use an input field having the following azimuthal vector distribution:
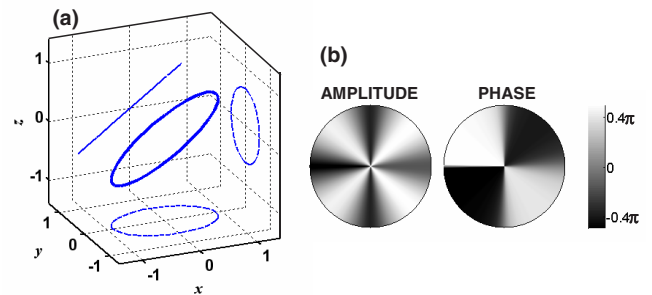


FIG. 2 (color online). (a) An example of a 3D state of polarization and its projections on three orthogonal planes. (b) The amplitude and phase distributions of the input field required to produce, at the focal spot, the polarization state shown in (a).

**(a)**



**(b)**
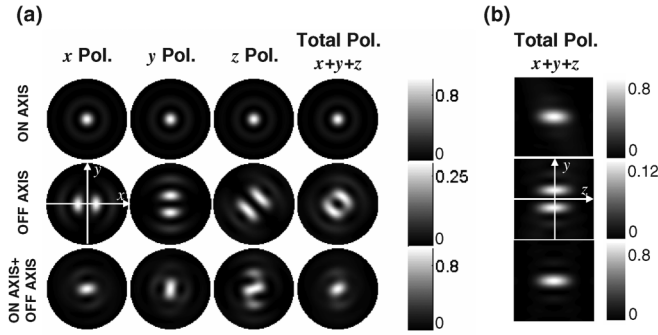
FIG. 3.   (a) Intensity distributions for on-axis, off-axis, and total components of the $x$, $y$, and $z$ polarizations in the focal plane ($x$-$y$) that correspond to an on-axis field having $E_x = E_y = E_z$ (see text for details). The scale bars refer to the last column normalized with respect to the peak of the total intensity distribution. All plots have a radius of 1 $\mu$m. (b) Intensity distributions for on-axis, off-axis, and total components in the $y$-$z$ plane for the total polarization. The dimensions of each square are 2 $\mu$m in the $y$ direction, as in (a), and 4 $\mu$m in the $z$ direction.

$$\Lambda (\beta) = \{\bar{\Lambda}^x + C_1^x \cos\beta\}\hat{\mathbf{x}} + \{\bar{\Lambda}^y + S_1^y \sin\beta\}\hat{\mathbf{y}}, \quad (9)$$

with $\bar{\Lambda}^x = \bar{\Lambda}^y = \frac{I_0^c(0)}{I_0^a(0)}E_o$, and $C_1^x + S_1^y = 2E_o$. Placing $\bar{\Lambda}^x = \bar{\Lambda}^y = 0$ in Eq. (8) removes the focused $x$ and $y$ components, and results in a $z$-polarized focal spot, and the special case of $C_1^x = S_1^y$ corresponds to a radially polarized input beam (and, hence, a circularly symmetric focal field). Furthermore, the off-axis $z$ components produced by the $C_1^x$ and $S_1^y$ harmonics cancel out, resulting in a circularly symmetric on-axis $z$-polarized focal spot. An input beam having a uniform radial distribution (NA = 1.3) would result in 44% of the input power focused to the on-axis $z$ polarization, while a radial distribution of the form $r\sin(0.5\frac{r}{f})$, for example, raises this percentage to 63%.

We present a specific example of the application of the principles outlined in this Letter in Fig. 3, using NA = 1.3, $\lambda = 800$ nm, and $f = 1.5$ mm. The azimuthal dependence of the input beam was chosen to produce an on-axis focused field having $E_x = E_y = E_z$ [Eq. (9), $C_1^x = S_1^y$], and the radial dependence of the input field has the form $r\cos(4.5\frac{r}{f})$ (resulting in $\frac{I_0^c(0)}{I_0^a(0)} = 0.8613$). It is clear that the off-axis components [second row in Fig. 3(a)] are weaker than the on-axis components [first row in Fig. 3(a)], and may be further discriminated against by placing a pinhole at the detector plane for spatial filtering. The difference between the on-axis and off-axis contributions are further highlighted by examining the field away from the focal plane. In Fig. 3(b) we plot the on- and off-axis components in the $y$-$z$ plane, and it is clear that the off-axis components contribute to the field away from the optical axis.

Although this technique was couched in the terms of the electric field vector, it can alternatively be presented in terms of the focused magnetic field vector [12]. Furthermore, a similar approach can be formulated for controlling the 3D Poynting vector in the focal spot. Finally, in contrast to a recent proposal for 3D polarization control [14], our technique does not require the use of a femtosecond light source nor the proximity of a metallic nanoprobe.

In conclusion, we have presented an approach to high-NA lens focusing that delivers prescribed 3D states of polarization to the focal spot. We analyze input fields that are separable in the radial and azimuthal variables, and find that only the low-order azimuthal spatial harmonics contribute to the on-axis field. We identify the harmonics that contribute to each on-axis polarization component individually. Therefore, by controlling the azimuthal-harmonic content of the input field, one may exercise full control over the focused 3D state of polarization.

---

*Electronic address: raddy@mit.edu

[1] J. J. Stamnes, *Waves in Focal Regions* (Adam Hilger, Bristol, 1986).
[2] *Handbook of Biological Confocal Microscopy*, edited by J. B. Pawley (Plenum, New York, 1995), 2nd ed.
[3] N. Huse *et al.*, J Biomed. Opt. **6**, 480 (2001); S. Quabis *et al.*, Appl. Phys. B **72**, 109 (2001); E. Engel *et al.*, *ibid.* **77**, 11 (2003); A. Bouhelier *et al.*, Appl. Phys. Lett. **82**, 4596 (2003); K. C. Toussaint, Jr. *et al.*, Opt. Lett. **30**, 2846 (2005).
[4] J. J. Macklin *et al.*, Science **272**, 255 (1996); T. Ha *et al.*, Phys. Rev. Lett. **77**, 3979 (1996); A. P. Bartko and R. M. Dickson, J. Phys. Chem. B **103**, 11 237 (1999); B. Sick, B. Hecht, and L. Novotny, Phys. Rev. Lett. **85**, 4482 (2000); I. Chung *et al.*, Proc. Natl. Acad. Sci. U.S.A. **100**, 405 (2003); M. A. Lieb *et al.*, J. Opt. Soc. Am. B **21**, 1210 (2004).
[5] L. Novotny *et al.*, Phys. Rev. Lett. **79**, 645 (1997); L. Aigouy *et al.*, Opt. Lett. **24**, 187 (1999); T. Ichimura *et al.*, Phys. Rev. Lett. **92**, 220801 (2004); J. M. Gerton *et al.*, *ibid.* **93**, 180801 (2004); N. Hayazawa *et al.*, Appl. Phys. Lett. **85**, 6239 (2004).
[6] T. Brixner and G. Gerber, Opt. Lett. **26**, 557 (2001); Chem. Phys. Chem. **4**, 418 (2003).
[7] K. Hoki *et al.*, J. Chem. Phys. **116**, 8799 (2002).
[8] A. LaPorta and M. D. Wang, Phys. Rev. Lett. **92**, 190801 (2004).
[9] K. Adelman *et al.*, Proc. Natl. Acad. Sci. U.S.A. **99**, 13 538 (2002).
[10] E. Wolf, Proc. R. Soc. A **253**, 349 (1959); B. Richards and E. Wolf, *ibid.* **253**, 358 (1959).
[11] D. Porter and D. S. G. Stirling, *Integral Equations* (Cambridge University Press, Cambridge, 1990).
[12] A. F. Abouraddy and K. C. Toussaint, Jr. (to be published).
[13] T. R. M. Sales, Phys. Rev. Lett. **81**, 3844 (1998).
[14] T. Brixner *et al.*, Opt. Lett. **29**, 2187 (2004).